Hindawi
Journal of Sensors
Volume 2022, Article ID 9996626, 20 pages
https://doi.org/10.1155/2022/9996626

*Research Article*

# Analysis of the Evolution of Sea Water Quality in the Spanish Coast from Satellite Images before and during a Confinement Period

**Mar Parra, Lorena Parra, Jose M. Jimenez, and Jaime Lloret**

*Instituto de Investigación para la Gestión Integrada de Zonas Costeras, Universitat Politècnica de València, Spain*

Correspondence should be addressed to Jaime Lloret; jlloret@dcom.upv.es

Received 5 January 2022; Accepted 25 August 2022; Published 7 October 2022

Academic Editor: Yuan Li



Satellite imaging, a form of remote sensing, can be used to analyse water quality, which must be monitored for proper and sustainable environmental management. This paper studies the effect of a sea traffic reduction in the Alboran Sea (Spain), analysing the changes in water quality before (from February 3rd, 2020) and during (until June 22nd, 2020) a confinement period. This was an unprecedented event in modern times and brought an interesting opportunity to study dynamics when the human impact is reduced. The study of these dynamics and the concentration levels with little human effect is important for environmental conservation purposes. We applied already existing indices using ArcGIS and ACOLITE to determine the following environmental parameters: colored dissolved organic matter (CDOM), suspended particulate matter (SPM), chlorophyll-a (Chl-a), and harmful algal blooms (HABs). Prequarantine concentration levels can reach up to 4 a(CDOM)440 (CDOM), 18 g/m$^3$ (SPM), and 100 $\mu$g/L (Chl-a). Most prequarantine days presented an increment in either concentration level or distribution from the day before. The effects a sudden human impact has on an ecosystem which experimented reduced human influence for months were shown. On the day before the said impact (June 12th), three of the parameters were barely detected with concentration levels of mostly 2 a(CDOM)440 (CDOM), 6 g/m$^3$ (SPM), and 25 $\mu$g/L (Chl-a), and sparse distribution. Afterwards (June 22nd), their levels went up to 4 a(CDOM)440 (CDOM), 14 g/m$^3$ (SPM), and 1000 $\mu$g/L (Chl-a) and were distributed near the ports. The results presented in this study show that the main drivers of change when human impact was reduced were climatologic events (such as storms). Nevertheless, the importance of the human facto can be seen through the CDOM, SPM, and Chl-a plume near port areas observed the day after port activity was reactivated, June 22nd.

## 1. Introduction

When talking about environmental importance, noncontinental water bodies are essential for life. The oceans and seas serve as a supply of resources and as a key place where important socio-cultural activities are developed. Algae are an important resource in fixing carbon dioxide (CO2), which can be highly beneficial in stopping and reversing climate change [1]. If we focus on organisms, seas and oceans have very high levels of biodiversity, which must be protected since it is already highly threatened [2]. Tourism is one of the main economic drivers on the coast, especially in areas with warm climates. Furthermore, the oceans are used daily to move goods across the planet, and they offer many resources, such as fishing and energy. For all these reasons, the adequate protection of the seas and oceans is highly important. Spill pollution, eutrophication, and microplastics are just some of the most pressing problems that plague our waters. Uncontrolled discharges from ships can cause high mortality in a specific functional group or even several of them, as well as eutrophication problems. However, even nutrients can be harmful at high levels since they can generate algal blooms. This increase in microalgae can lead to eutrophication, causing a significant drop in the level of oxygen in an area [3]. The need to follow these problems closely and quantify their effects is clear; nevertheless, the method to do so must be as sustainable as possible. We have to avoid mistakes that have been made in the past, such as inefficient,

high-cost monitoring, and incorrect management [4]. The main problem with the study of marine quality is that the marine environment is aggressive, any instrument used on it is subject to corrosion. Nevertheless, this is not a problem when using satellite imagery. The usefulness of remote sensing to monitor changes in the marine environment has been proved by various authors. It has been applied during the quarantine caused by the virus SARS-CoV-2, the quarantine which prompted this study. Furthermore, remote sensing is a more sustainable alternative than charting a boat to take measures.

Starting in March 2020, Spain went into an emergency state, which reduced and even stopped trafficking [5]. It brought the opportunity to study environmental parameters with a lessened human impact. Some authors [6] have already stated that the first reports from environmental changes during the confinement period were from water and air quality. Yunus et al. [7] observed a 15.9% decrease in suspended particulate matter (SPM) in Vembanad lake, caused by the lockdown, thus proving the effect business activities have on the lake. Another lake (Hussain Sagar) was studied by Wagh et al. [8]. They studied the levels of colored dissolved organic matter (CDOM), chlorophyll-a (Chl-a), and total suspended solids (TSS). The CDOM and Chl-a levels went down during the lockdown. The absence of traffic and the expected decrease in pollutants from rivers (due to the decrease in factory production) is an unprecedented event in recent times. Their impact on the marine environment can be determined by comparing the data before and during the quarantine.

The aim of this paper is the study of the changes which happened on the Mediterranean coast in the Andalusia region (Alboran Sea) during the quarantine caused by SARS-CoV-2. Other authors have already demonstrated the effect a confinement period had on the environment; nevertheless, there is no specific study for this area. The site will be studied before and during the quarantine period. To do so, the dynamics for CDOM, SPM, Chl-a, and harmful algal blooms (HABs), which are water quality indicators, will be studied. Satellite imagery will be used to compare the studied periods. To monitor these parameters from February 2020 to June 2020, a distinctive methodology combining the use of ArcGIS,ESRI [9], and ACOLITE, MUSEUM [10], software will be employed. The imagery for this study will be from the satellite constellation Sentinel-2, more precisely using the Sentinel-2A-treated images. Only one of the two satellites which compose the Sentinel-2 missions will be used to reduce the errors due to possible dissimilarities between them. With this study, areas of interest, which could be more sensitive to changes and interesting for future studies, could be found (for example, close to ports). Moreover, the information derived from this study opens remarkable possibilities for the sustainable monitoring of the oceans. In the recovery and restoration area of environmental sciences, it is very important to specify the state to which the environment should return. One of the possibilities for the standards to which the recovery is to be held is deriving them from areas with reduced human impact. An opportunity to analyze such an area arises with the quarantine; the dynamics and concentration values for the studied parameters could be of use for restoration planning. The data from the months after the beginning of quarantine show what would happen to a marine environment if all human activities stopped. Therefore, the results of this experience could be used for recovery and restoration purposes as well.

This paper summarises the work performed in the thesis degree of the first author published by Parra [11] and is structured as follows. The findings of other research groups and how they can be related to this study are presented in Section 2. Section 3 describes the process through which the results will be obtained. Afterwards, the results are presented in Section 4. In this section, there are subsections for each parameter studied. In Section 5, we present a discussion of the results, breaking them down to better explain them. Finally, Section 6 presents the conclusions, as well as the possibilities for the future on this topic.

## 2. Related Work

In this section, some cases in which Sentinel imagery has been used to monitor environmental parameters are explained. The focus is on those relative to the sea. All this information is submitted to prove the importance of monitoring sea parameters and the usefulness of remote sensing.

Toming et al. [12] proved the efficiency of Sentinel-2 MSI data to monitor lake water quality at a global and local scale in 2016. They compared in situ measures of CDOM, Chl-a, and dissolved organic carbon (DOC) with band ratio algorithms. They used both Level-1C (pretreated) images and Level-2A images they atmospherically corrected using Sen2Cor. They employed the green to red band ratio to estimate the CDOM, DOC, and water colour. Chl-a concentrations were calculated using the 705 nm peak. They realised the atmospheric correction reduced the band ratio algorithm correlation, thus indicating the need for better atmospheric correction. Nevertheless, the R2 (a parameter which indicates the correlation from 0-no correlation to 1-perfect correlation) values from comparing the in situ results with the calculated results were high for Chl-a, CDOM, and DOC. They concluded that Sentinel-2 MSI data would be the key in developing new water monitoring techniques and research. Moreover, Orlandi et al. [13] used imagery from the Sentinel-2 MSI sensor to map water quality indices. The bands used by them were visible and near-infrared, and they compared the results with in situ data. They measured Chl-a, turbidity, and TSS using fifteen images of the Pescara River estuary on the Adriatic Sea. The Level-1C images were run through two atmospheric correction programs, Sen2Cor and ACOLITE. The R2 for the turbidity model was over 0.95. Although the R2 for Chl-a was ideal, the model presented better results than the standard OC3 algorithm, which is used. They proved the usefulness of Sentinel-2 MSI data for coastal research and monitoring.

Caballero et al. [14] used Sentinel-2 imagery to monitor the southwestern Spanish coast. This experience was conducted during the first year Sentinel-2 imagery was available to the public. They collected in situ samples of TSS in the Cadiz Bay, Guadalquivir estuary, and Conil port. This was

done to later compare the results derived from the model to the empiric results from the samples. They used an algorithm that selected the most sensitive TSS-water reflectance relationship to calculate the concentration. It used the red (664 nm) and near-infrared (865 nm) bands; both models presented high $R^2$ values. They used atmospheric correction strategies as well, ACOLITE and POLYMER. The latter proved to be quite useful for removing sunglint. In conclusion, Sentinel-2 data turned out to be useful for TSS monitoring in medium to high turbidity waters.

Li et al. [15] calculated SPM concentrations from the last twenty-two years using old imagery and a model created with Sentinel-2. First, they chose between five state-of-art models by comparing their results to 79 in situ datasets from the studied estuary. The models were recalibrated as well to ensure consistency. Then, they applied the chosen model to old Landsat imagery from 1997 to 2019. They were able to determine the SPM fluxes and, among other findings, discover seasonal patterns. Focusing on refining the detection of SPM concentration levels, Liu et al. [16] used in situ measures and Sentinel-2 MSI images to develop a model which could calculate the SPM concentration levels. The sixty-eight hyperspectral measurements they used were from Poyang Lake, China. Half of the samples were used to calibrate the model, whereas the rest were used to validate it. The resulting models were applied to new Sentinel-2 imagery and compared to those from the Terra-Moderate Resolution Imaging Spectroradiometer (MODIS) B01. The models, which used B04 to B8A, explained 77-93% of the SPM concentration variation. The most accurate models were the ones that used B07 for high loadings and B04 for low loadings.

Focusing on HAB detection, Potes et al. [17] tested previous algorithms developed for the ENVISAT-1 with Sentinel-2 data. The study area was the Alqueva reservoir, Portugal. Moreover, they tested the effectiveness of the algorithms for the new MSI instrument for Chl-a, water turbidity, density, and concentration of cyanobacteria. Their results were compared to in situ sampling and the analysis of Chl-a associated with HAB in laboratories. The MSI sensor was able to detect HABs. The study conducted by Khalili and Hasanlou [18] tested up to fifteen different indices for HAB monitoring using Sentinel-2 MSI data. Specifically, the test they performed was aimed at the detection of red tide algal blooms. Different statistical parameters were calculated for each index, such as overall accuracy, type I and II error, area under the curve, and Kappa coefficient. The model that presented the best results considering the statistical parameters was $(B04 - B8A)/(B04 + B8A)$. Following this, Alba et al. [19] used Sentinel-2 imagery to monitor an algal bloom event. This algal bloom event occurred in San Roque lake, Córdoba, Argentina. The bands used to detect the HAB were B04 and B08. Moreover, they used B8A and B09 to discern the algae composition patterns. The results were positive and showed the potential Sentinel-2 MSI data has for monitoring bloom events in eutrophic lakes.

Some authors have studied the effect of the lockdowns from SARS-CoV-2 had on the environment. Focusing specifically on water quality, we find Cecchi [20] who studied the decrease in seawater contaminants in the Lagoon of Venice. They detected that volatile organic compounds (VOCs) as well as microplastics and other pollutants significatively decreased. From the studied compounds, 17 were not detected after the lockdown period, and the ones which were detected were 9 with an input which was not altered by the lockdown or with a stronger persistence. Furthermore, Silva et al. [21] studied both the air and water quality in Spain and Portugal during the lockdown period. The water transparency increased during that time, with a reported reduction in total suspended matter (TSM) of 17% from the month of February to March (when the lockdown started), of 37% from March to April, and of 53% from April to May. It is to be noted that TSM is related to SPM. These studies prove that the lockdowns caused by the SARS-CoV-2 had a relevant effect in seawater quality.

Therefore, all these authors proved the usefulness of Sentinel-2 for monitoring these parameters under normal circumstances. The usefulness of satellite imagery for environmental monitoring has been thoroughly proved. It is especially relevant for areas hard to monitor manually. The sea is one of those areas, which could benefit from the continued monitoring via remote sensing. Nevertheless, the SARS-CoV-2 quarantine presented an unprecedented opportunity to study dynamics and the effect a reduction on human impact could have. Combining remote sensing services and quarantine (which allows for the study of water quality dynamics without human impact in this area) creates an ideal situation for novel research on seawater monitoring. In this paper, the water quality of the Alboran Sea (south-west Mediterranean region) is studied through four parameters: CDOM, SPM, Chl-a, and HABs. The background of the methodology used for each parameter is described in Section 3.4 of Materials and Methods. The study developed by Silva et al. [21] deals with seawater quality in the Iberian Peninsula; nevertheless, they focus on Portuguese waters, whereas this study is centered on the waters between Andalusia and Morocco. A study of the effects on seawater quality caused by the SARS-CoV-2 quarantine has yet to be published for this area.

## 3. Materials and Methods

Now, we are going to show the background, as well as the technical aspects of this study. To better understand this, the section is divided into four subsections. First, some background is provided in order to show where the data comes from and why it was chosen. Next, the method used to obtain the data is shown. Afterwards, the process the data undergoes before applying the indexes is thoroughly explained. Finally, those indexes are described.

### 3.1. Background

*3.1.1. Spatial and Circumstantial Framework.* The quarantine, caused by a virus, began on the 14th of March 2020. That day, many restrictions (most of them on mobility) were issued in Spain. The return to a state similar to the one before quarantine (New Normality) was done gradually

through a process named deescalation. The quarantine was declared officially over on the 21st of June 2020, thus starting the New Normality. It was a state similar to that from before the quarantine, nevertheless, with social distancing and facemasks. We summarised the changes in the marine area brought by every step on the deescalation [22], in Table 1. All the restrictions lifted on every step of the deescalation were forbidden during the period between March 14th and the date indicated on the table. Recreational sailing and cruises were prohibited, and even though commercial transport was still allowed [23], it was slowed due to a reduction in personal and restrictions on other countries.

The study area is situated where the Mediterranean Sea meets the Atlantic Ocean. It is delimited by the Strait of Gibraltar on the west, Andalusia (Spain) on the north, and Morocco and Algeria on the south. It is an exchange area where Atlantic water, less dense, flows on the upper part of the water whilst the Mediterranean waters sink while flowing out [24]. The area, its coordinates, and the surface covered by the study can be seen in Figure 1.

*3.1.2. Selected Image Source.* The imagery used for this study is obtained from the Sentinel-2 satellite, launched by the European Space Agency (ESA) [25]. It is a mission in conjunction with the Global Monitoring for Environment and Security (GMES) initiative, named "Sentinel." The missions were created within the Copernicus framework, and their objective is to monitor the Earth. The Sentinel-2 mission is comprised of two satellites phased 180°, which offers a high revisit time, and covers latitudes from 84° N to 56° S. The satellites, which weight 1.2 tones, have enough propellant to work for 12 years, although their estimated lifespan is 7 years and 3 months. They are endowed with several instruments, the most remarkable one being the MultiSpectral Instrument (MSI), which works passively by collecting reflected sunlight. The products available to the public are the Level-1C, Level-1B, and Level-2A images. Level-1C images are used in this paper because they have undergone preprocessing (with a <12 m root mean square error) before being accessible to the public [26]. This process includes geometric and radiometric corrections with both spatial registrations and ortho-rectification. The global reference system ensures subpixel accuracy.

The Sentinel-2 products used for this paper are raster images for which the value of the pixel is the reflectance at different wavelengths. The wavelengths, what they depict, and their resolution (pixel size) for the bands used are noted in Table 2.

Although it was not created specifically for marine monitoring like Sentinel-3, the Sentinel-2 mission offers high-resolution optical imagery (which the Sentinel-3 mission does not). This is a crucial factor since, usually, the higher the resolution, the higher the price [27]. Nevertheless, Sentinel-2 offers high-quality imagery for free. Therefore, the images from the satellites belonging to this mission are more suitable for imaging techniques.

*3.2. Data Acquisition and Management.* The data used for this paper will be extracted from the Copernicus Open Access Hub [28]. In this webpage, data from all over the world can be accessed, from every Sentinel satellite, for free. The areas for each Sentinel-2A image are not big enough to cover the entire Andalusian Mediterranean coast; therefore, we will have to select all the images needed (four images, dividing the coast into four subareas). These areas will be selected to ensure the presence of data from all the Spanish Alboran coastline. The names of the subareas are marked with three letters by Sentinel-2A; the subareas selected are STF, SUF, SVF, and SWF. This area was chosen due to the usually high marine trafficking, which is usually present there. It is the metaphoric door to the Mediterranean Sea, the Strait of Gibraltar. Every ship coming from outside the Mediterranean Sea has to go through it. Therefore, it is a suitable area for the study of possible changes due to a quarantine.

As stated before, there are four subareas, each corresponding to different parts of the Alboran sea. The first day from which we have data is the 3rd of February, and we know Sentinel-2A has a return time of 10 days in this area. Therefore, the last day for which there are data is the 22nd of June, barely a day after quarantine finished. This makes a total of fifteen days, an average of three per month, of data. The subarea SWF has data for more days than those studied; this is since this subarea is in the limit between two runs from the satellite. Therefore, some data from this area will not be used due to the dates not matching.

*3.3. Data Treatment.* This subsection is divided to understand the process better. Nevertheless, it can be summarised in the scheme presented in Figure 2. This scheme follows the workflow of this study. First images were obtained from the website. Afterwards, they were treated with both ArcGIS, ESRI [9], and ACOLITE, MUSEUM [10]. Finally, the results were displayed using ArcGIS.

*3.3.1. Pretreatment.* The images obtained from the Sentinel webpage had already been through the pretreatment mentioned in the previous subsection. Nonetheless, they still needed to be further processed before some of the indices were calculated. The Sentinel and Landsat software [10], developed by the Royal Belgian Institute of Natural Sciences, was used for this step. This software was built specifically for marine and inland water bodies monitoring and has been proved to be useful for Sentinel-2 before [29]. It uses the light reflectance from each pixel and applies formulas to the images treating them as if they were matrices. Among the processes it performs, the most important is the atmospheric correction; this is done using the dark spectrum fitting approach by Vanhellemont [30]. Moreover, it can apply indexes and existing formulas to derive parameters with their corresponding values. ACOLITE works with a specific configuration that can be altered by creating .txt files with new settings. Currently, it works with Python 20190326.0.

It is to be noted that part of the main treatment was applied when running the ACOLITE scripts for the pretreatment, specifically for the Chl-a and SPM indices. Nevertheless, this step was just the beginning for the HAB and

Table 1: Effects of the deescalation for the marine area.

| Phase 0 | Phase 1 | Phase 2 | Phase 3 |
|---|---|---|---|
| Quarantine conditions | Exceptions in some autonomic communities for marine transport. 50% occupation with 2 meters between seats, 100% occupation in cabins for people living together | Recreational fishing allowed Recreational sailing only within the territorial unit | Passengers allowed to embark ferries Recreational sailing allowed within the national territory |

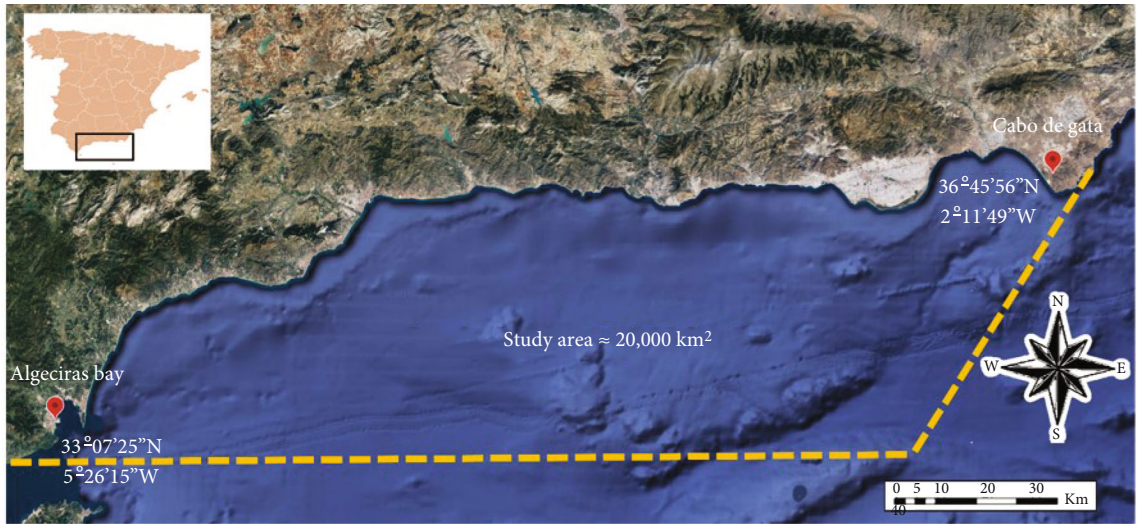


Figure 1: Study area, sea delimited by the discontinued line.

Table 2: Bands used and their characteristics.

| Band name | Wavelength (nm) | Description | Resolution (m) |
|---|---|---|---|
| B03 | 0.560 | Green | 10 |
| B04 | 0.665 | Red | 10 |
| B06 | 0.740 | Vegetation red edge | 20 |
| B08 | 0.842 | Near infrared (NIR) | 10 |
| B8A | 0.865 | Vegetation red edge | 20 |

CDOM indices. It was done to optimise the use of this software instead of running two different scripts, one for the pretreatment and one for the main treatment. Although ACOLITE can represent HAB, the index used in this paper applies a different equation.

The first step for the pretreatment of the images used for the HAB index was to merge the images for B04 and B8A. It was done using the ArcGIS software, ESRI [31], more precisely the "Mosaic To New Raster" tool [32], which can be found in the Data Management Tools. It was done for both B04 and B8A for each day. The images generated are the ones that will be used later for the main treatment for HAB. Said treatment is explained in detail in the next subsection.

*3.3.2. Main Treatment.* The ACOLITE script for each day was a modification of the default script to which new commands were added and some old commands were modified. The input and output were selected, as well as the 12 w parameters (among them were the indices). Moreover, it was specified for the results to be obtained in .tif format and not to generate .png files. The 12 w parameters chosen were Rrs_560, Rrs_665, spm_nechad2016, and chl_re_moses3b740.

The Rrs_560 and Rrs_665 images were used for the CDOM index, and before calculating it, it was needed to combine them. It was done following the same method as for the HAB images, combining the B03 and B04 images in this case. The main treatment for the Chl-a and SPM was done by ACOLITE, and the files generated by spm_nechad2016 and chl_re_moses3b740 were ready to be analysed. For the main treatment for HAB and CDOM, another ArcGIS Tool was used. In this case, the chosen tool was one that is useful for many remote sensing applications; the "Raster Calculator" [33]. Raster files can be interpreted as large matrices in which each pixel is one number from the matrix. The Raster Calculator applies a specified formula to the matrix represented by the raster. Several indices, explained in the following subsection, were used.

*3.4. Used Indices.* In this subsection, the indices used to estimate the levels of CDOM, SPM, Chl-a, and HAB are described. This subsection has been divided into four brief parts to ease the understanding thereof. Each of them deals with one of the indices.

*3.4.1. CDOM.* CDOM [34] is the part of dissolved organic matter which can be detected via optical techniques. It is

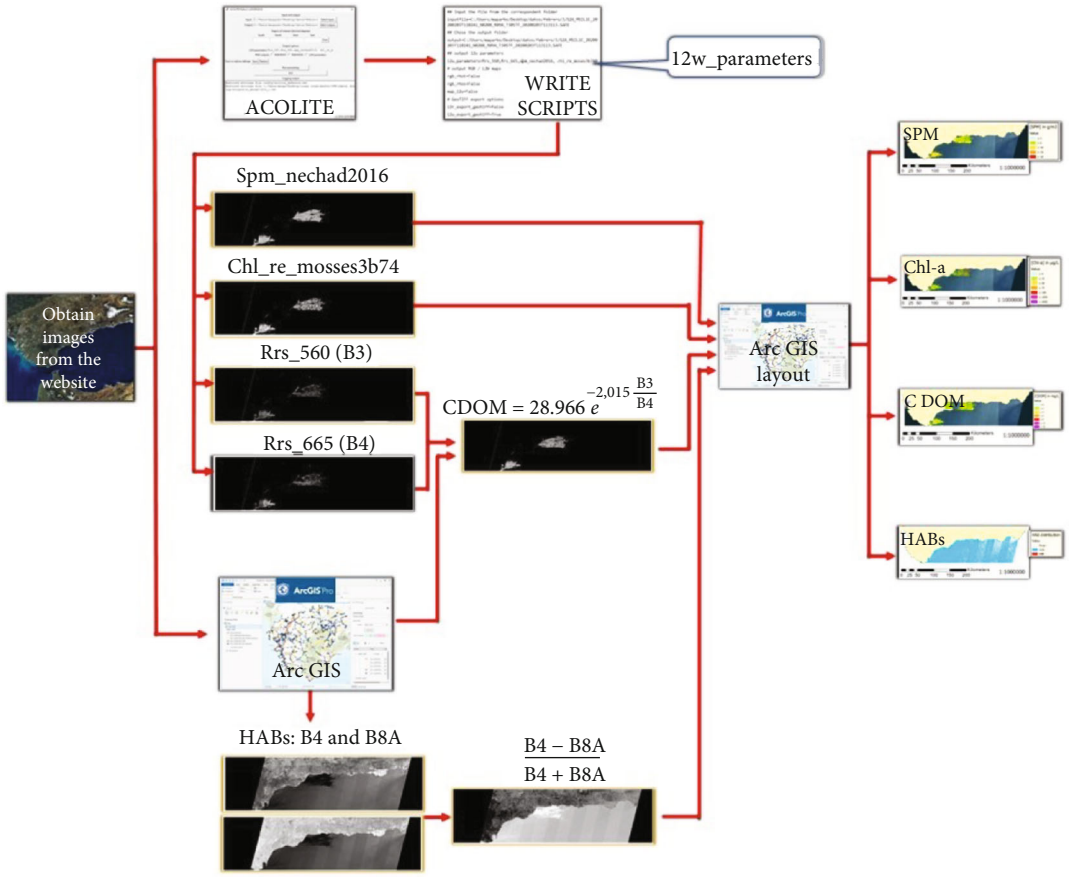


Figure 2: Scheme of the methodology.

humic-rich and affects the light levels in the water column, therefore, affecting the entire ecosystem. It peaks naturally during spring and intense weather conditions such as storms and hurricanes. It is due to these events causing massive overland flows. Nonnatural causes for peaks include human activities such as sewage treatment plant discharge and agricultural and farming runoff.

Chen et al. [35] developed several models for the remote sensing of CDOM and Chl-a concentration levels in 2017. They used Sentinel-2 data and calibrated it with data from field measurements. The tests were conducted on Lake Huron, China. Twelve models were developed and tested for CDOM alone, four of them proving to be useful. Later on, in 2020, another study conducted by the same team used one of them, which used B03 and B04 [36]. It is the index used for our CDOM identification, the formula to estimate the CDOM levels using B03 and B04 as seen in

$$\text{CDOM (a(CDOM)440)} = 28.966 \cdot e^{-2.015 \cdot (B3/B4)}. \quad (1)$$

The results from this equation were the CDOM concentration levels in absorbance at 440 nm for each pixel, a(CDOM)440. This is the most used unity for CDOM measurements. It is to be noted that each pixel was $10 \times 10$ meters in real life due to both bands used for this index having that resolution.

*3.4.2. SPM.* SPM [37] is linked to CDOM because both increase with runoffs and both being sediments. It modifies the colour and transparency of water as well. Nevertheless, SPM is associated with bacteria and metallic contaminants. Some human causes for an increase in the SPM levels include offshore wind farms, dams, sand extraction, transport of pollutants… Natural causes for SPM variation include water velocity and hydrological alternation [38].

The SPM levels were derived from the raster files generated by ACOLITE. The program used the formula developed by Nechad et al. [39], seen in its empirical formula in Equation (2). In which $T$ is the turbidity (SPM in g/m$^3$), $A$ and $B$ are coefficients which depend on the wavelength used (2383.49 and 0, respectively, for 842$\lambda$). The $R^2$ for this method using the selected wavelength is 0.889. The $X$ is the water-leaving reflectance, obtained from the 842 $\lambda$. The equation with the parameters for this case can be seen in Equation (3).

$$T\left(\frac{g}{m^3}\right) = A(\lambda) \cdot X(\lambda) + B(\lambda), \quad (2)$$

$$T\left(\frac{g}{m^3}\right) = 2383.49 \cdot B8 + 0. \quad (3)$$

The formula has been proved useful by Chapalain [40], who used it for a study on SPM dynamics and characteristics

on the French coast. First, the program applied an atmospheric correction to the images; next, using the NIR images, the concentration (in g/m$^3$) was calculated for each pixel. This step was done when running the script on ACOLITE, and there was no need for ArcGIS to generate this data, only to display it. The equation for this parameter was not introduced; it was applied automatically by ACOLITE. Therefore, it is not noted in this study.

*3.4.3. Chl-a.* As stated by Pérez-Ruzafa et al. [41], Chl-a indicates the trophic state of waters since it is a proxy for phytoplankton biomass. High Chl-a levels indicate eutrophication, a state for which dissolved oxygen becomes a scarce resource, thus affecting the entire ecosystem. This increase in phytoplankton happens when there is a high nutrient load. The Chl-a levels in the sea are usually lower than in lakes and coastal lagoons; nonetheless, they increase with weather events such as storms since overland flow increases the nutrient load.

In the case of Chl-a, the results were obtained from ACOLITE as well. The formula used was first postulated by Moses et al. [42]. The said formula usually employs the reflection at a wavelength of 708 nm as a reference. Nevertheless, it can be specified for it to use the one at 740 nm (B6), as seen in Equation (4), for which $Rx$ is the remote sensing reflectance for the band at $x$ nm. This equation was chosen because the concentrations were slightly higher when employing the 740 nm band as reference. When determining harmful concentrations, it is better to overestimate them. Moreover, since the objective is to compare the changes between different days, it is better to have higher values; the changes can be more notable.

$$\mathrm{Chl_a}\left(\frac{\mu g}{L}\right) = \left[113.36 \cdot \left\{\left(R_{B4}^{-1} - R_{B6}^{-1}\right) + R_{B6}\right\} + 16.45\right]^{1.124}. \tag{4}$$

Many studies have used the equation developed by Moses et al. [42] in 2012. In 2019, Warren et al. [43] used it to monitor Chl-a levels in a comparative study. Moreover, it was used by Phalevan et al. [44] when they retrieved Chl-a from Sentinel-3 and Sentinel-2 imagery using machine learning in 2020. For our study, the concentration levels were calculated for each pixel and were shown in $\mu$g/L. The formula was applied automatically by ACOLITE during the pretreatment. ArcGIS was only used to display the data.

*3.4.4. HABs.* HABs [45] disrupt the entire marine ecosystem and can cause eutrophication. They can impact the local economy, food security, human health, and tourism. The warming and acidification of the seas, as well as deoxygenation (all caused by climate change), increase the possibility of a HAB. Moreover, they can be caused by high nutrient loads after extreme climatic events such as storms or hurricanes.

For HABs, the formula used was the one determined to be the best for this type of measure by Khalili and Hasanlou [18]. This equation resulted from research with an extensive background; the likes of which include the work developed by Carvalho et al. [46] to detect *Karenia brevis* blooms along the west coast of Florida and the Gulf of Mexico. Moreover, they also applied the results from the research conducted by Matthews et al. [47] in which the HABs were studied through the use of Chl-a levels. The formula developed by them and used in this paper is different from the ones above. It shows the pixels that have a higher difference between Red and Vegetation Red Edge bands. It is to be noted that B8A had a smaller resolution than B04. Therefore, their result had the smallest resolution (20 m). This index was calculated using the Raster Calculator Tool ARCGIS DESKTOP [33] using

$$\mathrm{HABs} = \frac{\mathrm{B4\text{-}B8A}}{\mathrm{B4\text{-}B8A}}. \tag{5}$$

The results for this index ranged from -1 to +1 due to the nature of its equation; they are dimensionless. For pixels where the value for B04 was significantly bigger than for B8A, the results were close to 1. Whereas for pixels where the value for B8A was significantly bigger than for B04, the resulting pixels were close to -1. In pixels where the values for B04 and B8A were similar, the resulting pixel had a value close to 0. According to Khalili and Hasanlou [18], HAB-laden waters present bigger differences for B04 and B8A than normal seawater. Therefore, values closer to 1 represent HABs, whereas low positive values are water. Clouds are white; therefore, the reflectance for B04 and B8A is similar for them. Therefore, numbers very close to 0 (both positive and negative) are clouds, and low positive values represent water. Since land is of no concern for this study and will be represented using another layer on the map, we do not need to specify another category for discerning land.

## 4. Results

The results are presented now for each of the parameters monitored in the area and period specified. This section has been divided into five subsections to achieve a clean presentation of the results. The representation of the data is explained in the first one. The second section deals with the changes in CDOM. Next, the evolution in SPM is presented. Moreover, the spatial-temporal changes in Chl-a are shown in the third subsection. Next, the distribution of HAB is presented in the fourth subsection. It is important to note that in this section, the results are presented, and their possible causes are mentioned. The next section (Discussion) details and analyses the causes, drivers, and dynamics and summarises them.

*4.1. Data Analysis and Representation.* The resulting images have been displayed using ArcGIS. Four results have been obtained per day using their pixel values to colour the images. The CDOM, SPM, and Chl-a images correspond to their concentrations, whereas the HAB images represent their presence or absence. All the images have the "≤0" range to indicate water due to the nature of the equations and to eliminate possible errors (negative values).

For the CDOM, SPM, and Chl-a indexes, the true colour images are represented underneath. These images place the clouds and help interpret the results. In order to make sure it rained whenever clouds are present in the pictures, weather tables are checked [48]. The values do not represent the magnitude of the storm at sea, in any case. Nevertheless, they can assert the presence of rain. The effect rain has on concentration levels has to be taken into account to identify the cause of increasements during the quarantine period. It is important to note that the SPM and Chl-a concentration levels (measured g/m$^3$ and $\mu$g/L, respectively) cannot be considered equivalent due to the Chl-a concentration levels in $\mu$g/L presenting a difference in concentration values one thousand times smaller than the SPM ones. The choice in units is due to Chl-a levels being very low at sea.

It is to be noted that the period studied in this paper was very cloudy, which is to be expected from a winter-spring time interval. The quality of the data is not the same for every studied day. Some days are cloudier than others, and the area which can be studied is reduced, which affects the distribution. Not all the weather is visible; some clouds look like water due to them being very low. Nevertheless, the images have been thoroughly studied, and the results derived from them are presented in this section, broken down for an easier understanding. In February, the second day, the 13th, presents a storm covering its sky. There are clouds on all three days; nonetheless, those clouds are small and localised for the first day, the 3rd. For the third day, the 23rd, they only cover the western part of the Alboran Sea. On March, the first day, March 4th, the sky is clear. Nevertheless, on March 14th, clouds cover the western part of the Alboran Sea in a similar way to the image from February 23rd. Finally, for the third day, Mach 24th, the sky is almost fully covered; even though the eastern part of the sea seems visible, it is covered by low clouds, in which the imaging techniques are difficult. When observing April, the large clouds covering the second day, April 14th, can be distinguished. Moreover, on the third day, April 24th, some clouds cover the area. Not only they cover the parts which look white, low clouds were present during this day. The only day with complete data is the first day, April 4th. This day presents some errors since the satellite images used were slightly compromised; it can be seen on the right side of the image. It shows lines in which the values are much lower than expected compared to those around them, which is an error due to the source data (the satellite images) being compromised. It can be seen in most of the images; nonetheless, the effect is more notable in this one. May is the first month in which all three days can be studied without major clouds interfering. The first day, May 4th, has a clear sky, as does the third day, May 24th. The second day, May 14th, presents some clouds on the western part of the Alboran Sea, close to the Strait of Gibraltar. Half of the study area had entered phase 1 on May 14th, and next, for the third day, May 24th, all the area was on phase 1. Finally, June 2nd is hard to study due to the clouds that seem similar to those on April 23rd; nevertheless, small gaps between clouds can be analysed. For June 12th, the situation is similar, although a small area in the west can be seen. The third day, June 22nd, presents a clear sky. It is important to note that on June 1st, the entire area entered phase 2; on June 8th, it entered phase 3, and on June 21st, it entered the New Normality.

*4.2. CDOM.* In this subsection, the results concerning the concentrations of CDOM are presented. They can be seen in Figure 3.

The CDOM concentration levels for February are presented in Figures 3(a)–3(c). Most values on February 3rd were lower than 2 a(CDOM)440. Their distribution does not seem to reveal any pattern other than it being slightly more prominent near the clouds. It is important to note that these concentrations correspond to data taken in the middle of winter and before the quarantine started. Natural CDOM peaks usually happen during spring [34]. Next, for February 13th, the results are more difficult to interpret since there were many clouds. Nevertheless, the data shown on the gaps between clouds present higher concentrations of CDOM. The concentrations for those areas, higher than that of the 3rd, can be explained through the storm that can be seen in the weather tables [48] and the port activity. Even though some clouds are present on February 23rd, most of the data can be interpreted. An overall increase respecting the concentrations from February 3rd can be seen. Concentrations from 2 to 4 a(CDOM)440 can be found in the southeastern part of the area.

The CDOM concentration levels for March are presented in Figures 3(d)–3(f). The values from March 4th show concentrations from the 0 a(CDOM)440 to 2 a(CDOM)440 range and from the 2 to 4 a(CDOM)440 range. The distribution shown by them is similar to the one present on February 23rd (Figure 3(c)). This could easily be explained due to the rains experienced the week before, as seen in the weather tables [48], and the port activity. The conditions already present ten days before are maintained; heavy rains hit the peninsula the week before March 14th, the date on which quarantine started. Moreover, some clouds only allow the eastern part of the Alboran Sea and the coastline to be studied on this date. Some parts of the sea present concentration values over 4 a(CDOM)440. Furthermore, there seems to be higher concentrations nearshore which could be caused by the overland flow due to the storm. For March 24th, not much can be analysed since clouds cover most of the sea. The CDOM concentration peaked, reaching values of even 8 a(CDOM)440. This can be explained due to the intense weather conditions that week, which created massive overflows and then the currents pulled the matter together in one direction. Furthermore, spring started, which is the time of the year in which CDOM levels naturally peak [34], possibly explaining that peak.

The CDOM concentrations for April are displayed in Figures 3(g)–3(i). Even though the image error concentration values of 0 to 2 a(CDOM)440 can be seen in almost all the sea. Furthermore, concentration levels of 2 to 4 a(CDOM)440 can be seen in the eastern part of the sea, similar to those in Figures 3(c) and 3(d). The previous week was dominated by heavy storms, as seen in weather tables [48], explaining the high concentrations of nearshore. For April

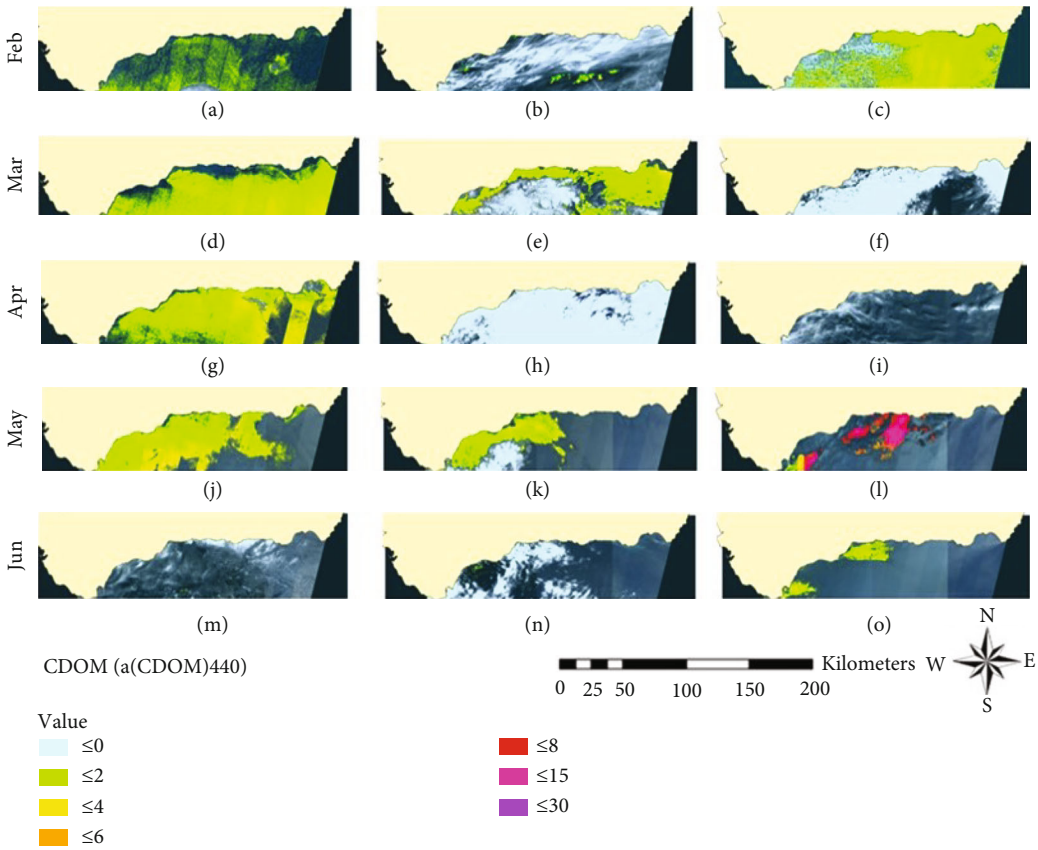


Figure 3: CDOM concentrations. Each map represents (a) February 3rd, (b) February 13th (c) February 23rd, (d) March 4th, (e) March 14th, (f) March 24th, (g) April 3rd, (h) April 13th, (i) April 23rd, (j) May 3rd, (k) May 13th and (l) May 23rd, (m) June 2nd, (n) June 12th, and (o) June 22nd.

14th and April 24th, there is not much to be analysed. They both show concentration levels up to 6 a(CDOM)440 in small areas, which could be analysed between clouds. The weather tables [48] show storms throughout the month, explaining the difficulty in obtaining good satellite imagery and the high concentration levels.

For May, the CDOM concentrations are presented in Figures 3(j)–3(l). The concentration levels for May 4th show a distribution close to the coast with higher concentrations at the centre-western offshore waters. It can be explained due to the storms from the week before [48]. Following, for May 14th, it is important to remark the lower presence of storms the week before [48]. Thus, we can see how the CDOM distribution is closer to the coast. This reduction on the week where there were no storms further proves that they are most likely the main cause of peaks on this month and April. In the week previous to the third day this month, May 24th, there were storms again. Moreover, temperatures started to increase [48]. The results presented in Figure 3(l) show the highest CDOM concentrations of all. It is certainly a CDOM peak, which is to be expected around spring [34], and can be caused by the storms combined with the temperature increase. Those parameters can affect the physicochemical properties and its ecosystem, thus making the degradation of CDOM slower.

Finally, the concentrations of CDOM for June are shown in Figures 3(m)–3(o). For June 2nd, only some small gaps between clouds can be analysed. Nevertheless, most of the values for those areas are on the 0 to 2 a(CDOM)440 and 2 to 4 a(CDOM)440 concentration ranges. It means a drastic decrease considering the values for May 24th (Figure 3(l)). Nonetheless, ten mostly dry days went by between both images, and storms are the main drivers of change for these parameters when the human impact is reduced. The impact reduction linked with other parameters such as temperature, wind, and the physicochemical characteristics of the sea may have caused the decrease, which was possible due to the port activity being stopped. The next day, June 12th, shows no CDOM in the eastern part of the Alboran Sea. Moreover, the western side presents very small concentrations in areas where the clouds open and the sea can be studied. After this week, marine transportation was allowed on all the national territory, and passengers were allowed to embark on ferries. Finally, on June 22nd, two very distinctive plumes can be seen heading east. One of them comes from the Algeciras (left) port area, while the other comes from the area around Malaga (centre). Moreover, the concentrations for this date present a more similar distribution of the ranges 0 a(CDOM)440 to 2 a(CDOM)440 and 2 a(CDOM)440 to 4 a(CDOM)440

than any other image. Furthermore, it presents concentration levels up to 14 a(CDOM)440.

*4.3. SPM.* This subsection deals with the results concerning the concentrations of SPM. They can be related to the concentrations of CDOM since their causes are similar [34]. Nevertheless, SPM levels can increase due to other causes. They can be seen in Figure 4.

For February, the concentration levels can be seen in Figures 4(a)–4(c). The SPM levels are low and close to the shore and clouds for February 3rd. This distribution does not correlate to the CDOM distribution, thus indicating the cause for them is different. In comparison to CDOM levels, these are more localised, especially nearshore. Most of the concentration levels for this day are below 6 g/m$^3$. Even though not much can be analysed for February 13th, the concentration levels for the small areas between clouds certainly present higher values than the previous day, up to 18 g/m$^3$. It correlates with what happened to CDOM, thus proving they were caused by the same factor. For February 23rd, all the visible water presents concentrations higher than 2 g/m$^3$. Some parts of the southeastern area present concentrations up to 10 g/m$^3$. Moreover, areas close to the clouds and close to the coast have SPM levels up to 14 g/m$^3$ and even 18 g/m$^3$, which is the highest SPM concentration level for the entire studied period and is presented on two of the three studied days that month.

The next month to be studied is March, during which the quarantine started. The SPM concentration levels for March can be seen in Figures 4(d)–4(f). For March 4th, a distribution similar to the one observed on February 23rd (Figure 4(c)) can be observed. Nevertheless, concentrations seem to peak near Malaga port, with levels up to 18 g/m$^3$. The port activity is a likely cause of this peak. Concentrations are also high nearshore in Cabo de Gata and Almeria (top right corner). Surprisingly enough, concentrations are not as high in Algeciras port, although the currents can be an important factor. On March 14th, the day quarantine started, the concentrations peaked both in the east and west but lowered at the Malaga port. The areas which can be seen between clouds in the west show concentrations on the 2 to 6 g/m$^3$ and 6 to 10 g/m$^3$ ranges. In the east, values peak around Almeria and Cabo de Gata, reaching concentrations up to 14 g/m$^3$ and even 18 g/m$^3$. Although they reach the shore near Cabo de Gata, they seem to not due to the effect of clouds. It may be caused by dust transported by wind since the week previous to that day had been dry, and dust being carried offshore is a natural cause for high SPM concentrations at sea [34]. For March 24th, not much can be said. The small gaps between clouds present low concentration levels, unlike CDOM concentrations for this date.

The results from April are presented in Figures 4(g)–4(i). The concentration levels for April 3rd are higher on the eastern side of the Alboran Sea. It is unfortunate since it is the area for which the file was corrupted and could not compute the entire image. Nevertheless, the increased concentration can be seen. Most of the concentration values for that area reach 10 g/m$^3$. Concentrations are higher nearshore, going up to 14 g/m$^3$, reinforcing the possibility of the peaks being due to dust carried through the wind; therefore, not caused by port activity. Concentration levels of CDOM were also higher on the southeastern side for this date, although they were not present nearshore. SPM does seem to be present nearshore for most of the images in which it is detected. For April 13th, some small gaps between clouds can be seen, for which the average concentration seems to be in the 10 to 14 g/m$^3$. The next studied day, April 23rd, presents lower concentrations, most of them on the 2 to 6 g/m$^3$ range. Changes for this month may have to do with hydrological conditions caused by the storms on the weeks previous to them [48].

The concentration levels for SPM in May are shown in Figures 4(j)–4(l). The concentration levels for May 3rd seem to be the consequence of those in April still. SPM presence is no longer on the eastern part of the Alboran Sea, and now, the higher values are on the western side. Although most values are on the 2 to 6 g/m$^3$ range, values from the 6 to 10 g/m$^3$ and 10 to 14 g/m$^3$ ranges can be seen offshore. The week previous to this date presents high precipitation levels [48]. CDOM presented high concentration levels on that area for this date, indicating a massive overland flow caused by storms, which has already gone far into the sea and carries SPM. For May 13th, the concentrations seem to have lowered, although they are close to the western side as well. Their distribution is similar to the CDOM distribution for this date, reinforcing the possibility of natural causes. The concentration levels for May 23rd seem to have lowered to mostly values from 2 to 6 g/m$^3$. Nonetheless, SPM has spread in distribution, covering areas not covered on May 13$^{th}$, which may have to do with winds. It is important to note that on May 18th, the entirety of the study area entered phase 1. The weather most likely caused all changes for this month.

June (Figures 4(m)–4(o)) is the last month to be studied. Most of the data for June 2nd cannot be analysed due to the clouds covering the sea. Nonetheless, for the small gaps in which the imaging techniques could be run, the values presented are mostly on the 2 to 6 g/m$^3$ range. On this date, all of Andalusia was already on phase 2. On June 8th, the area of interest entered phase 3. Although data from June 12th cannot be analysed as well as data from other days, it shows low concentration values. Most of them are in the 2 to 6 g/m$^3$ range and do not cover the full extent of the opening between clouds. Finally, on June 22nd, a day after the end of quarantine, the concentration values peaked. It is interesting to note that their distribution is very similar to the distribution of CDOM for this date. They are higher near the Algeciras port and the Malaga port. Especially on the Algeciras area, for which values on the 10 to 14 g/m$^3$ range can be seen. On this date, the other concentration levels have values on the 2 to 6 g/m$^3$ and 6 to 10 g/m$^3$ ranges.

*4.4. Chlorophyll-a (Chl-a).* In this subsection, the results for the Chl-a levels on the Alboran Sea are presented in Figure 5. High Chl-a levels can be naturally caused by storms and high nutrient loads [38], presenting a correlation with high CDOM and SPM.

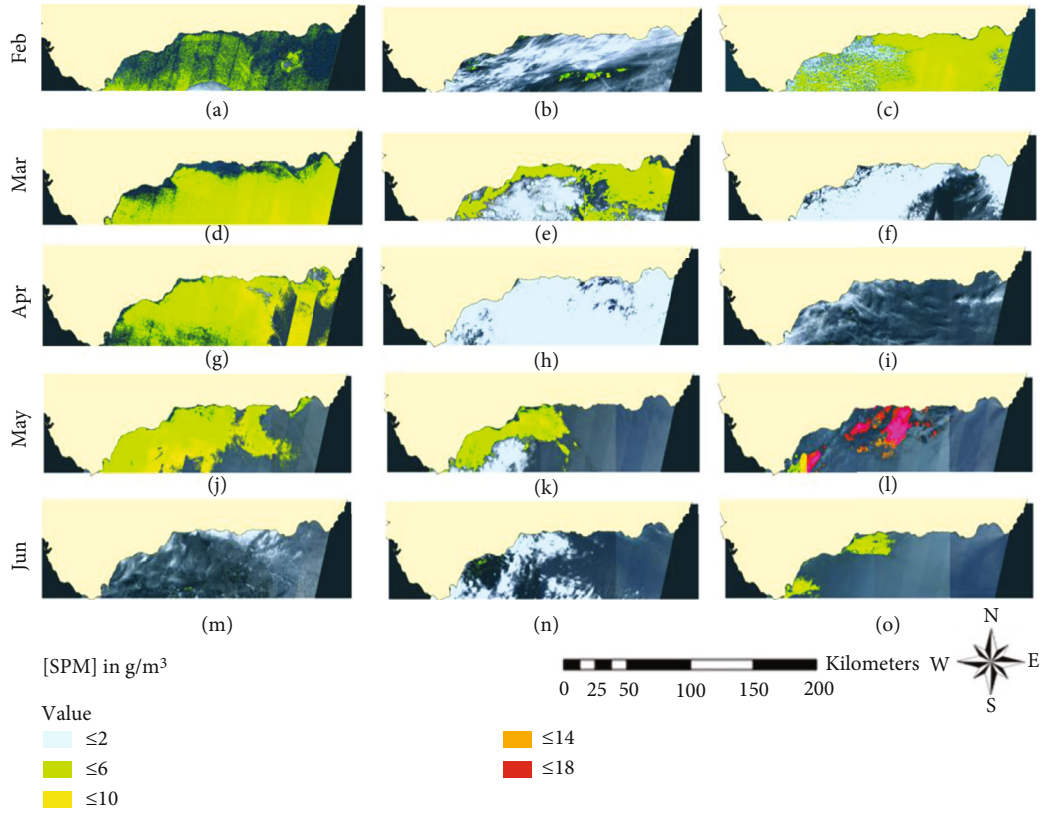


Figure 4: SPM concentrations. Each map represents (a) February 3rd, (b) February 13th, (c) February 23rd, (d) March 4th, (e) March 14th, (f) March 24th, (g) April 3rd, (h) April 13th, (i) April 23rd, (j) May 3rd, (k) May 13th, (l) May 23rd, (m) June 2nd, (n) June 12th, and (o) June 22nd.

The concentration levels for February can be seen in Figures 5(a)–5(c). The Chl-a levels for February 3rd present mostly concentrations lower than 50 $\mu$g/L. Nonetheless, this date presents higher concentrations near the Malaga port and the Strait of Gibraltar, where the Algeciras port is located. Concentrations present in these areas go up to 100 $\mu$g/L. Chl-a is detected in the entirety of the area of study. For February 13th, not much can be studied. Nevertheless, the areas visible through the clouds present concentration levels with most values lower than 25 $\mu$g/L. Although concentration levels did not change much, the coverage increased. On February 23rd, both higher concentrations and a larger presence of Chl-a can be seen. Most concentration levels are lower than 50 $\mu$g/L. Nonetheless, there seem to be more peaks on the 50 to 75 $\mu$g/L and 75 to 100 $\mu$g/L ranges than for the first day this month. Since storms those weeks were not intense, the increment was most likely caused by port activity.

For March, the Chl-a concentration levels are shown in Figures 5(d)–5(f). March 4th shows a scenario similar to February 24th (Figure 5(c)), although the Chl-a levels close to the coast seem to have reduced. Most concentration levels present values lower than 50 $\mu$g/L for this date. Nevertheless, there are more areas with concentrations up to 100 $\mu$g/L than for the previous studied day. For this date, CDOM presented higher concentrations as well. For March 14th, the concentrations seem to have lowered; most of them fall on the 0 to 25 $\mu$g/L range. Nonetheless, their distribution thickens on the eastern side of the sea, which correlates to SPM and CDOM concentration levels increase for this date. It is possible that the dust which could have caused the SPM unusually high levels contained a high proportion of nutrients. It is important to note that this date is the day the quarantine started. Next, March 24th is difficult to interpret. The only data available is from small gaps between clouds, the concentration levels for these gaps present values on the 25 to 50 $\mu$g/L range. This is probably caused by the storms which hit Andalusia during this period. CDOM concentrations were high for this date as well.

Next comes April; its Chl-a concentration levels are shown in Figures 5(g)–5(i). For April 3rd, concentration levels mostly on the 0 to 25 $\mu$g/L range can be seen throughout the entire area. The said area presents concentration levels on the 25 to 50 $\mu$g/L range, although less than for the other range. Similar to SPM and CDOM, the higher concentration levels for this date are on the eastern side of the Alboran Sea. In this case, there are some areas for which the concentration gets to 75 $\mu$g/L. The week before this date presented rains; this increase could be caused by those storms. Next, April 13th presents little to no data. The points for which concentrations were calculated between clouds present concentrations on the 0 to 25 $\mu$g/L range mostly and some on the 25 to 50 $\mu$g/L range. The spatial distribution of the Chl-a cannot be studied for either this date or

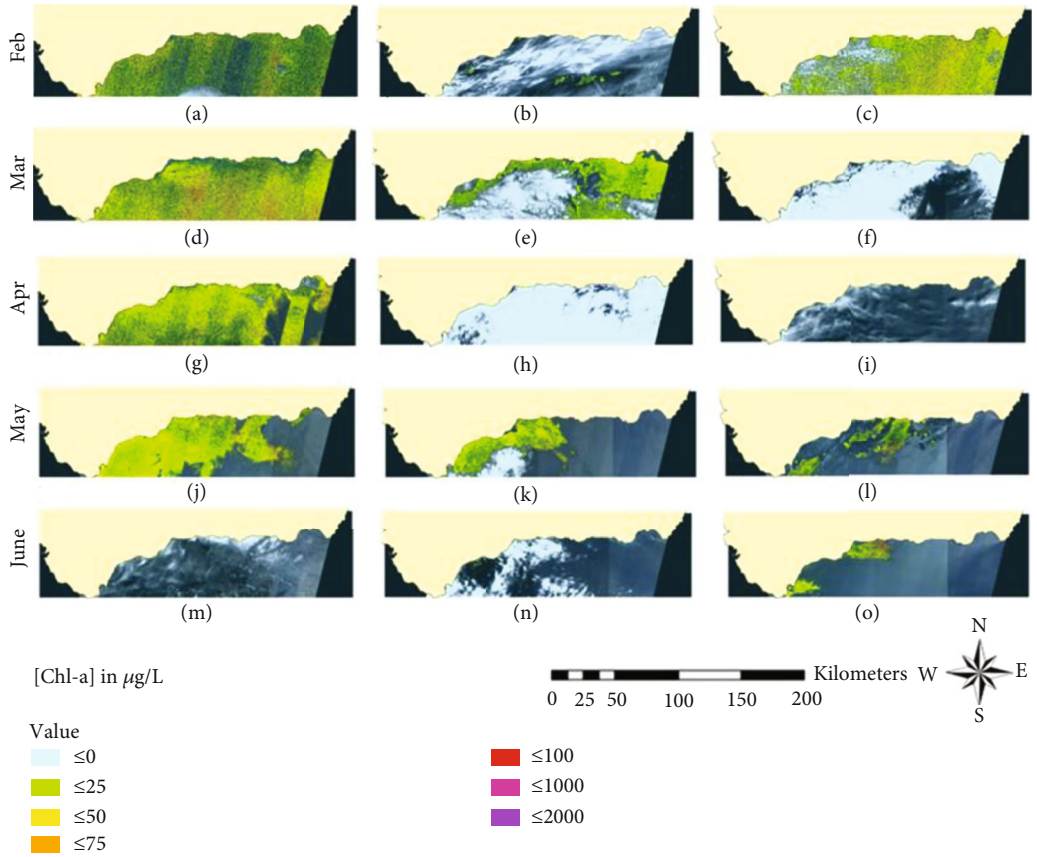


Figure 5: Chl-a concentrations. Each map represents (a) February 3rd, (b) February 13th and (c) February 23rd, (d) March 4th, (e) March 14th, (f) March 24th, (g) April 3rd, (h) April 13th, (i) April 23rd, (j) May 3rd, (k) May 13th, (l) May 23rd, (m) June 2nd, (n) June 12th, and (o) June 22nd.

the next. Then, the concentration levels which can be studied for April 23rd present mostly values on the 0 to 25 $\mu$g/L range. Contrary to April 13th, this date presents concentrations higher than 50 $\mu$g/L, on the 50 to 75 $\mu$g/L range. This sudden increase most likely had to do with the storms, and the massive overland flows caused by them.

Then, the next month analysed is May. The Chl-a concentration values for the said month can be seen in Figures 5(j)–5(l). The first studied day, May 3rd, presents concentration levels mostly on the 0 to 25 $\mu$g/L range. Nonetheless, near the Algeciras port, concentration levels increase to the 25 to 50 $\mu$g/L range. Furthermore, some values near the coastline on the central and eastern parts of the sea present concentration levels up to 75 $\mu$g/L. These levels are not only present there but also on the plume on the east. For May 13th, the concentration levels have mostly reduced both in magnitude and dispersion. During this period, there were fewer storms, which could explain these values. The concentration levels for Chl-a present for this day correlate to CDOM and SPM as well. Increases in concentration levels for all these parameters can be naturally caused by storms. Therefore, this retreating behaviour can be interpreted as the consequence of a storm since it was the main driver of change without human impact. On May 18th, all of Andalusia entered phase 1. The week previous to May 23rd was dominated by heavy rains [48], explaining the higher concentration values presented in the central area for this date. These concentrations increased up to 100 $\mu$g/L and, on some parts, even 1000 $\mu$g/L and 2000 $\mu$g/L. It is an unprecedented peak for the period studied for this paper. Moreover, it correlates with the CDOM peak.

Finally, the last month is June. The Chl-a concentration levels for this month can be seen in Figures 5(m)–5(o). The values for June 2nd were taken a day after phase 2 started in Andalusia. It presents concentrations up to 100 $\mu$g/L for the small gaps between clouds, which could be caused by precipitations. On June 8th, all of Andalusia entered phase 3. Therefore, the values for June 12th correspond to this period. Recreational fishing was permitted, and recreational sailing was allowed within the territorial unit [22]. Concentration levels and distribution on the gap on the western side of the Alboran Sea are low and sparse. The Chl-a levels show almost no Chl-a compared to the levels before the quarantine (Figure 5(a)). Finally, on June 22nd, barely a day after the instauration of the New Normality, two plumes can be seen. One of them seems to come from the Algeciras port, while the other comes from the Malaga Port. Chl-a concentration levels for the Algeciras port plume are on the 0 to 25 $\mu$g/L and 25 to 50 $\mu$g/L ranges mostly. In contrast, Chl-a concentration levels for the Malaga port plume reach 1000 $\mu$g/L and present many values on the 75 to 100 $\mu$g/L range.

*4.5. HABs.* The analysis of the distribution for HABs throughout the studied period is different from the analysis for CDOM, SPM, and Chl-a. There were only three HAB episodes in the five months studied for this paper. Nevertheless, Figure 6 shows the results for the days which presented HABs.

The first and biggest bloom is on February 3rd (Figure 6(a)). The HAB distribution corresponds with the Chl-a distribution for that date. The values here show a clear HAB, big enough to cover the entire Alboran Sea. The first week of February presents temperatures higher than usual [46], which added to the usually high nutrient content in this season [47] and could have caused the bloom. It happened before the quarantine. The second bloom happened on April 4th (Figure 6(b)), close to the Strait of Gibraltar. It does not match with high Chl-a, CDOM, or SPM levels, which could indicate the algal class [49]. The bloom, nonetheless, seems to come from the strait, probably being caused by a nutrient load entering the Mediterranean Sea. The last noticeable bloom is on May 3rd (Figure 6(c)). It matches up with high Chl-a concentrations as well as the presence of CDOM and SPM. Therefore, it is similar to the bloom on February 3rd. It is most likely due to the high nutrient load present on the sea after the storms which hit Andalusia the week before [48]. Both this HAB and on April 4th happened during phase 0.

## 5. Discussion

Next, we are going to discuss the results. It has been divided into five subsections to improve the presentation of the observations which have been made. The first one summarises the dynamics observed in the study area and compares the results to those obtained from other studies done in similar areas before the quarantine period. The second subsection deals with the effects of the reactivation of ports. The problem when observing HABs is explained in the third subsection. Localised tendencies are explained in the fourth one. The fifth subsection presents the limitations the technology used has. It is to be noted that this information is key to derive the conclusions for the next section.

*5.1. Summary of the Observed Dynamics.* The observed dynamics are presented in Figure 7. Increases are shown in colour red, whereas decreases are shown in colour green. The days for which the concentration levels were similar to the days before are shown in yellow. Moreover, the HABs are represented in red. The rains are represented in different shades of blue depending on their intensity (darker for heavier rain). The first day for CDOM, SPM, and Chl-a is marked in red to indicate their presence.

February, a winter month, presents some light to moderate precipitations [48], and an increasing or maintaining trend for CDOM, SPM, and Chl-a. These concentration levels can be explained by the rains. Spring started in March, a month for which the concentrations of Chl-a seem to be a follow-up of the storms in February. SPM presents a peak not related to storms during this month; on the 14th, CDOM does too. Nevertheless, they show different distributions and may be caused by human factors. March 14th is the day quarantine started.

During the quarantine, the month of April is hard to analyse due to the intense precipitations present in this period. The high CDOM, SPM, and Chl-a values can be explained by those storms. On May 13th, all the concentration levels are lowering; nevertheless, after another intense precipitation event, the CDOM and Chl-a concentration levels rose. Finally, during June, without human activities or storm periods, the CDOM, SPM, and Chl-a concentration levels were lower, although June 22nd, the day after quarantine ended, presents a sudden increase in all three parameters.

It is to be noted that most days that presented increases during the quarantine happened after an intense storm period. Moreover, the quarantine period presents more days with a decreasing trend, especially for May and June, after the rainy season (this season being the last week of March and the month of April). Two out of three HABs correlate with high CDOM, SPM, and Chl-a concentration levels; the outlier may be caused by a nutrient load entering from the Atlantic Ocean. Furthermore, on June 22nd, barely a day after the New Normality was established, an increase can be observed. The data after the quarantine period is not further studied because this study was conducted in June.

Furthermore, to better understand the dynamics, we present three graphics showing the distribution as well as the peak concentration of CDOM, SPM, and Chl-a for each of the studied days. Figures 8–10 present the aforementioned values. For five of the studied days, the distribution cannot be determined due to the high cloud coverage; for those days, it is not represented to avoid misinterpretations since it cannot be stated with accuracy. The days for which was not possible to study the distribution are March 24th, April 13th, April 23rd, June 2nd, and June 12th. The days lockdown started and finished are underlined on the $X$-axis.

Figure 8 presents the dynamics for CDOM. It can be seen that previous to the lockdown, the highest value was lower; this is due CDOM peaking naturally during spring [34]. The peak on May 23rd comes right after an intense storm period, which is a natural cause for CDOM peaks. What can be observed during the confinement period, though, is the decrease in distribution. Most prelockdown days (except February 2nd) present a high distribution.

When comparing to the results from other authors, Organelli et al. [50] measured the CDOM levels on the NW Mediterranean Sea for two years. For the months studied in this paper, the dynamic observed is an increase in spring and a decrease in June. Later on, El Hourany et al. [51] studied the CDOM levels on the eastern Mediterranean Sea, close to the Nile's mouth. They observed high values from February to April, and they decreased in May and June. Nonetheless, they used a slightly different wavelength (412 nm instead of 440 nm as in this study). Therefore, their results prove the existence of a peak in spring, as has been stated before [34] and as shown in these results. Nevertheless, the numerical data cannot be compared.

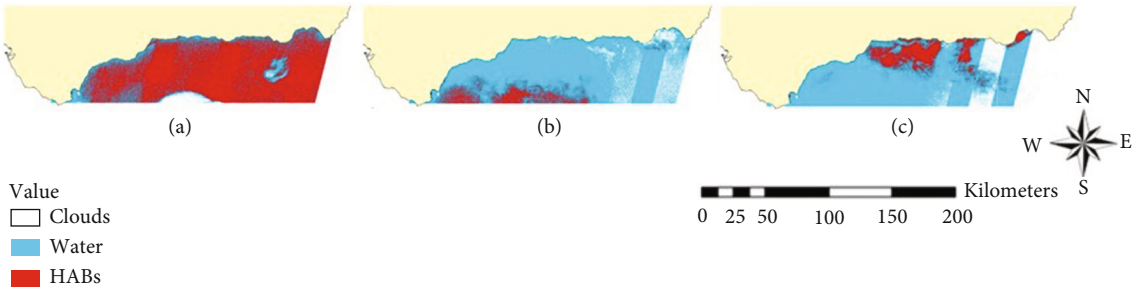


Figure 6: HABs during the studied period. Each map represents (a) February 3rd, (b) April 3rd, and (c) May 3rd.

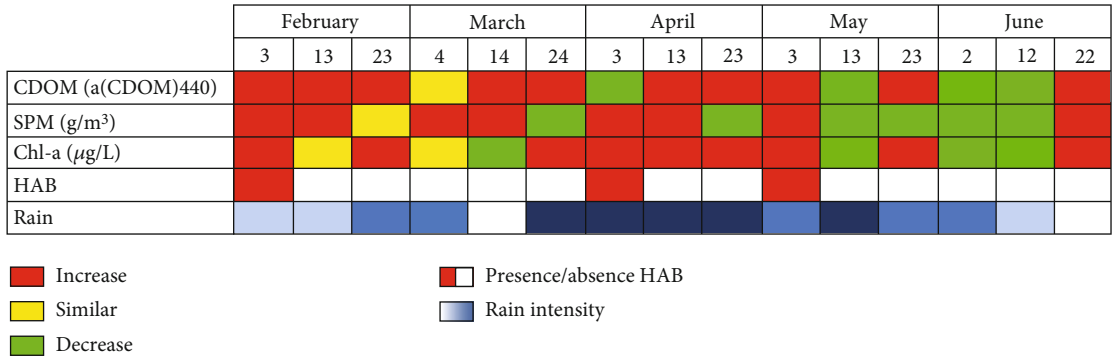


Figure 7: Summary of the dynamics and peaks.

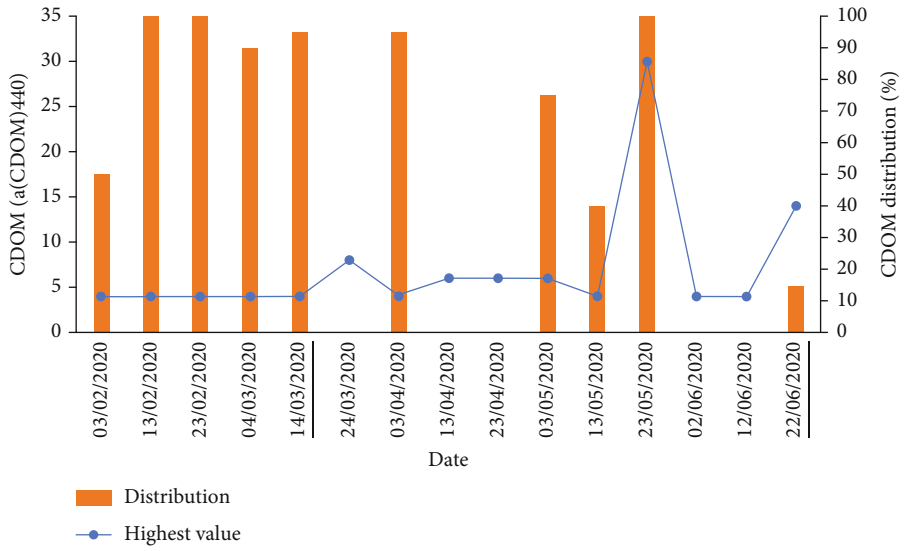


Figure 8: CDOM peaks (line) and distribution (columns).

In Figure 9 the evolution of SPM can be observed. This is the parameter which presents the clearest results with both the distribution and its peaks decreasing during the lockdown period. All of the days during lockdown present lower peak values than those from the prelockdown period (except for February 2nd). The distribution decreases for most days as well.

Other authors who have studied SPM values include Cresson et al. [52], who studied the particulate organic matter levels and composition in the Bay of Marseilles, the NW Mediterranean Sea. The units they used (μg/mg) can be considered equivalent to the ones used in our paper (g/m$^3$), although seawater does not have a density of exactly 1 kg/1 dm$^3$. The values presented are higher than those calculated for the studied period.

Figure 10 shows the evolution of Chl-a distribution and concentration peaks during the studied period. The values decreased at the beginning of quarantine, although they

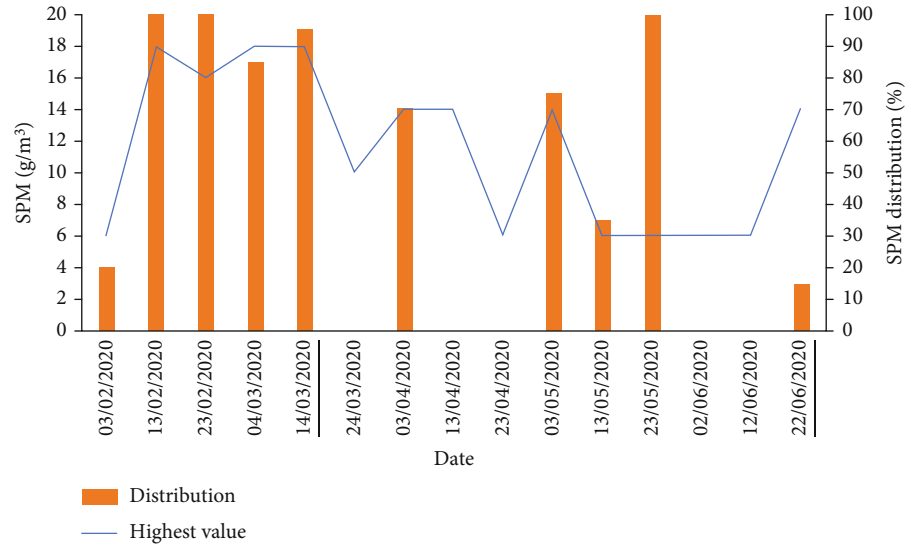


Figure 9: SPM peaks (line) and distribution (columns).

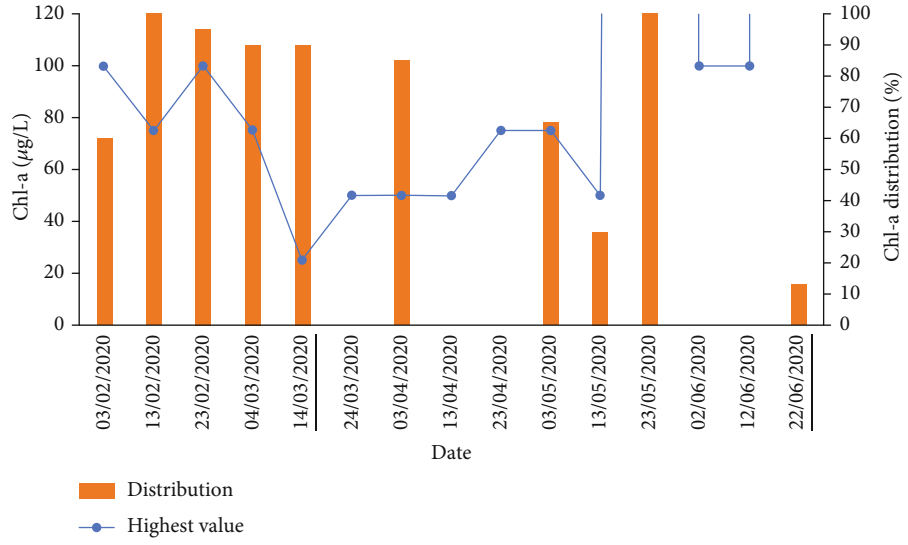


Figure 10: Chl-a peaks (line) and distribution (columns).

peaked in spring, as it is natural for Chl-a [41]. The distribution lowered as seen in the days for which it was possible to study it.

To analyse the values of Chl-a, they can be compared to the work conducted by Fabres et al. [53]. As for SPM, the values can be compared, although the density of the water does not make the units completely equivalent. It can be seen that for the days in May, the values on regular years are higher than those for our studied period.

One thing becomes clear when observing Figure 7, the longer the quarantine period had been going on, the lower the concentration levels. Even during spring, for which many of them peak naturally, Slonecker et al. [34], Kang et al. [38, Pérez-Ruzafa et al. [41], and Gobler [45]. Concentration levels before the lockdown are high and not caused by storms since they were lower than those in spring. Nevertheless, the days with high concentration levels during the quarantine period are right after or during storm periods.

*5.2. Effects of the Port Reactivation.* The quarantine period is characterised by the reduction of port activity. When comparing the March-June period in 2019 and 2020 for the Algeciras Port, Autoridad Portuaria de la Bahía de Algeciras [54], we can observe the shift in dynamics. The passenger traffic decreased an 82.06%, whereas industrial vehicles present a 12.78% reduction. Overall, 42.39% fewer vessels entered the port, and the gross tons shift reaches 13.79%. Furthermore, March et al. [5] showed the rapid port reactivation in Spain in their study.

As shown in Figures 3–5, the concentration levels for CDOM, SPM, and Chl-a increased the day after the

reactivation of port activities. It is important to note that on this date, many restrictions regarding marine transportation had been lifted [22]. Taking this into account and observing both peaks near important ports, it is easy to assert the cause. The plumes are most likely caused by a human factor, the revitalisation of marine transportation. According to Vessel Finder, Historical AIS Data Services [55], the traffic density in the seaport of Algeciras was very high on June 22nd. Although the Malaga port does not seem to present many ships, they were big ships, two of them around 25.000 gross tons [56].

Considering the weather conditions [48], this peak in concentration levels cannot be explained by weather conditions. No storms were present the weeks previous to this date. The most likely explanation is the human impact after the reactivation of port activities. This event generated an anthropogenic impact. As stated before, the plumes seem to have their origin in the two main ports in this area. Although there are more ports in the study area, those two are the most important, with higher trafficaffluence. We see the Algeciras port on the right, while on the left, we see the Malaga port. These are the two most important ports in the area of interest. It is important to note that the plumes have similar behaviour; they drift to the east. It can be explained due to the currents which affect the area; they go from the Atlantic Ocean towards the Mediterranean Sea [57].

Ports are areas with high concentration levels for pollutants [58]. Sipelgas et al. [59] observed the total suspended matter levels on several Estonian harbours for 10 years using MERIS imagery. The behaviour they observed is similar to the one present on the day after the end of quarantine.

*5.3. HABs Problematic.* The HABs detected in this paper are those associated with high biomass levels. They are dangerous for many reasons, such as eutrophication, gill damage which could kill fish, and food web disruption [60]. They can be caused by toxic or nontoxic species. Nevertheless, it is important to monitor these events due to their negative consequences. Nevertheless, HABs not associated with high biomass cannot be detected with this method. Moreover, HABs are short-spanned phenomena [19], which explains why only three HABs have been observed in this experience. Nonetheless, this does not mean that only three HABs happened during the studied period. The HABs represented in this paper may not be all the blooms that happened during this period. The return time of the images used (10 days) is a problem when monitoring HABs.

It is important to note that even though for June 22nd all concentrations are high near the Algeciras port and the Malaga port, a HAB cannot be seen. Nevertheless, after just one day of marine trafficking, it is to be expected. Ouellette et al. [61] identified, in 2016, the main challenges of remote sensing for marine monitoring purposes. They were reliability, continuity, institutional barriers, knowledge gap, resolution, and coverage. HABs need a high continuity. Later on, in 2018, Burford et al. [62] noted the usefulness of remote sensing for covering large areas and its lack in a high temporal frequency, thus resulting not ideal for HABs monitoring. Shi et al. [63] included as a challenge the low-time frequency remote sensing presents.

*5.4. Localised Tendencies.* Several tendencies were observed during the studied period. However, most of them are exposed in Section 4.1. This section deals with those with a more localised extension.

We observe a tendency of higher concentration levels near the Cabo de Gata and Almeria, especially notable for SPM on March 14th (Figure 4(e)). It may be due to the intensive agricultural use of the land in the area [64]. Moreover, this tendency is present during the quarantine, which could be explained since agriculture was not stopped. Pollutants get to the sea through agricultural runoff, a phenomenon that has been studied since the 70s [65]. Like Griffin et al. [66] in 1982, many authors have remarked the impact agricultural runoff has on water quality. Nowadays, the removal of pesticides and pollutants from agricultural runoff is being studied [67].

Furthermore, several days for several parameters present higher concentration levels near the port areas. Besides June 22nd (explained on 4.2.), the most notable one is on March 14th for SPM (Figure 4(e)). It is normal to have high pollution levels near port areas [58], as explained in Section 4.2. Therefore, this peak could be explained by an increase in marine transport activity. The date for these unusually high values near the port is that of the beginning of quarantine, indicating a high activity of the previous days. This activity was caused most likely by many ships returning to the port due to the pandemic.

In addition, the rivers present in this area are either short or wadis. Therefore, it is to be expected not to find a tendency near their river mouths except for when it rains (explained in Section 4.1). Long rivers, with a high flow all year long, carry more pollutants and can affect the sea, as in the Bohai Sea [68].

*5.5. Limitations of the Used Technology.* The analysis conducted in this paper yields information useful for seawater quality monitoring. Nevertheless, it would be better to be able to have data from more days. Combining Sentinel-2 and Landsat-8 like other researchers have done before would reduce the time between two datasets. Therefore, the monitoring would be more thorough. Statistical analyses could be run (since there are not enough days studied to run a trustworthy $t$-test to compare results before and during quarantine).

The resolution for some of the bands used is lower than for others, thus creating results with different resolutions. Unfortunately, given the available technology, this cannot be mended. The only option would be to use imagery from other satellite missions. Nonetheless, their cost would be higher than the ideal for this type of study.

There are parameters for which there are not any established indices. ACOLITE only has built-in formulas for SPM, turbidity, Chl-a, HABs, NDVI, particulate backscattering, and temperature. Therefore, other indices cannot be monitored with the proposed system. The obvious solution would be to create those indices, which could be done by

studying the behaviour of those parameters to check which bands would work better and then compare the new indices with real in situ data.

It could be argued that the reliability of remote sensing using satellite imagery is based on contact measures. Nevertheless, the plausible error caused by the calibration is always the same, unlike for contact measures, for which the error changes as the sensor is corroded. Moreover, remote sensing offers periodical results and is less expensive and more sustainable than charting a boat to take contact measures.

## 6. Conclusions

The study of the water quality has been achieved by analysing satellite imagery using ArcGIS, ESRI [9], and ACOLITE, MUSEUM [10], software to produce indices for a series of environmental parameters. The results (concentration levels) for these parameters have been analysed to study tendencies and possible drivers of change. Furthermore, they have been compared with each other and with weather tables [48].

For several of the days studied, the CDOM, SPM, and Chl-a concentrations peaked simultaneously and showed a similar distribution, presumably due to the storms on the week before each date, causing a massive overland flow. Moreover, the concentrations lowering and dispersing after a storm can be observed in several of the days. Nevertheless, the prequarantine data present more days with high concentrations even though the storms were less intense. The port was reactivated one day after the quarantine was finished, 22nd July. CDOM, SPM, and Chl-a concentrations peaked this day near the Malaga port and the Algeciras port, proving the impact of human activity in an environment that had been undisturbed for several months.

For CDOM, 100% of the days until March 14th present concentration levels higher or similar to those from the previous one. All of them have concentrations on the 0 to 2 a(CDOM)440 and 2 to 4 a(CDOM)440 ranges, covering most of the studied area. Whereas for the quarantine period, a 55% of the days present higher or equal concentration levels than the previous one. For SPM, the contrast is even starker, with 33% of the days during the quarantine presenting increasing tendencies. Meanwhile, all the prequarantine levels (100%) presented an increase. Furthermore, the highest peaks, 18 $g/m^3$, are presented on February 13th, February 23rd, March 4th, and March 14th. Chl-a levels present a difference that is not as extreme as for SPM; nevertheless, it is higher than for CDOM. An 80% of the studied prequarantine days show higher or similar Chl-a concentrations to the day before (March 14th being the outlier), whilst 67% of the quarantine days present it (although with lower distributions). The Chl-a peak happened during one of the intense storm periods in May. Nonetheless, another peak happened on February 23rd with levels up to 100 $\mu$g/L.

February 3 presents the biggest HAB and high Chl-a and CDOM concentrations showing a distribution similar to the HAB. It also presents SPM distributed nearshore. The HAB was most likely caused by the high temperatures [48] and the nutrient-rich waters [68] and influenced the Chl-a and CDOM readings. Two more HAB have been observed, one of them, on May 3rd, related to the storms. The other HAB, on April 3rd, does not correlate to the CDOM, SPM, and Chl-a concentration levels or distribution. This HAB is close to the Strait of Gibraltar and could have been caused by nutrient-rich waters entering the Mediterranean Sea. There were only 3 observed HABs during the period. Nevertheless, the most extended one was on February 3rd.

The possible future projects are split into two directions. The first direction would be the continuation of monitoring marine environments. First, other indices could be tested, even some original indices comparing their results to the observed in situ values (from buoys). Moreover, this could be done for other places rather than just the Alboran Sea, and other image sources like Landsat-8 could be used as well. Another future study could be the use of satellite imagery for environmental monitoring during the SARS-CoV-2 quarantine applied to other ecosystems (forests, lakes, wetlands…). It would be interesting to check the effect a prolonged underexposure to human activities could have on these environments. Moreover, it could help us understand their dynamics and processes. Furthermore, wireless sensor networks (WSN) could be employed to improve and verify the data (especially in nonaggressive, hard-to-access environments). By contrasting the data from satellite imagery to that from sensors, the results could be more precise. WSNs have been proved useful for the monitoring of the hydrosphere previously. There are low-cost sensors for monitoring turbidity and SPM, Matos et al. [69]. Areas of interest, like seagrass areas, have already been monitored by multisensory buoys part of a WSN [70] and could benefit from further monitoring.

## Data Availability

Publicly available datasets were analysed in this study. This data can be found here: https://scihub.copernicus.eu/dhus/#/home.

## Conflicts of Interest

The authors declare no conflict of interest.

## Authors' Contributions

All the authors have contributed equally towards the conceptualisation, methodology, development, and conception of the experiments and with reagents/materials/analysis tools. All authors have contributed in writing the paper. All authors have read and agreed to the published version of the manuscript.

## Acknowledgments

This research was funded by the European Union through the ERANETMED (Euromediterranean Cooperation through ERANET joint activities and beyond) project ERANETMED3-227 SMARTWATIR; by Conselleria de Educación, Cultura y Deporte with the Subvenciones para

la contratación de personal investigador en fase postdoctoral, grant number APOSTD/2019/04; and by Universitat Politècnica de València through Program PAID-01-20 and PAID-10-20.

## References

[1] V. Paul, P. C. Shekharaiah, S. Kushwaha, A. Sapre, S. Dasgupta, and D. Sanyal, "Role of algae in CO 2 sequestration addressing climate change: a review," in *Proceedings of Renewable Energy and Climate Change*, pp. 257–265, Maninagar, India, 2019.

[2] C. C. O'Hara, J. C. Villaseñor-Derbez, G. M. Ralph, and B. S. Halpern, "Mapping status and conservation of global at-risk marine biodiversity," *Conservation Letters*, vol. 12, no. 4, p. e12651, 2019.

[3] J. E. van Beusekom, "Eutrophication," in *Handbook on Marine Environment Protection*, M. Salomon and T. Markus, Eds., vol. 1 and 2, pp. 429–445, Springer International Publishing, New York, USA, 2018.

[4] J. D. Nichols and B. K. Williams, "Monitoring for conservation," *Trends in Ecology & Evolution*, vol. 21, no. 12, pp. 668–673, 2006.

[5] D. March, K. Metcalfe, J. Tintoré, and B. J. Godley, "Tracking the global reduction of marine traffic during the COVID-19 pandemic," *Nature Communications*, vol. 12, no. 1, pp. 1–12, 2021.

[6] M. Coll, "Environmental effects of the COVID-19 pandemic from a (marine) ecological perspective," *Ethics in Science and Environmental Politics*, vol. 20, pp. 41–55, 2020.

[7] A. P. Yunus, Y. Masago, and Y. Hijioka, "COVID-19 and surface water quality: improved lake water quality during the lockdown," *Science of the Total Environment*, vol. 731, p. 139012, 2020.

[8] P. Wagh, J. M. Sojan, S. J. Babu, R. Valsala, S. Bhatia, and R. Srivastav, "Indicative lake water quality assessment using remote sensing images-effect of COVID-19 lockdown," *Water*, vol. 13, no. 1, p. 73, 2021.

[9] ArcGIS, ESRI, "ESRI. ArcGIS Pro Website," 2020, https://pro.arcgis.com/es/pro-app/latest/get-started/install-and-sign-in-to-arcgis-pro.html.

[10] Museum Acolite, 2020, https://odnature.naturalsciences.be/remsem/software-and-data/acolite.

[11] M. Parra, "Analysis of the evolution of sea water quality in the Spanish coast from satellite images before and during the quarantine caused by COVID-19, [M.S. thesis]," Universitat Politècnica de València, 2020.

[12] K. Toming, T. Kutser, A. Laas, M. Sepp, B. Paavel, and T. Nõges, "First experiences in mapping lake water quality parameters with Sentinel-2 MSI imagery," *Remote Sensing*, vol. 8, no. 8, p. 640, 2016.

[13] M. Orlandi, F. Silvio Marzano, and D. Cimini, "Remote sensing of water quality indexes from Sentinel-2 imagery: development and validation around Italian river estuaries," in *Proceedings of EGUGA*, p. 19808, Vienna, Austria, 2018.

[14] I. Caballero, F. Steinmetz, and G. Navarro, "Evaluation of the first year of operational Sentinel-2A data for retrieval of suspended solids in medium-to high-turbidity waters," *Remote Sensing*, vol. 10, no. 7, p. 982, 2018.

[15] P. Li, Y. Ke, J. Bai, S. Zhang, M. Chen, and D. Zhou, "Spatio-temporal dynamics of suspended particulate matter in the Yellow River Estuary, China during the past two decades based on time-series Landsat and Sentinel-2 data," *Marine Pollution Bulletin*, vol. 149, p. 110518, 2019.

[16] H. Liu, Q. Li, T. Shi, S. Hu, G. Wu, and Q. Zhou, "Application of sentinel 2 MSI images to retrieve suspended particulate matter concentrations in Poyang Lake," *Remote Sensing*, vol. 9, no. 7, p. 761, 2019.

[17] M. Potes, G. Rodrigues, A. M. Penha et al., "Use of Sentinel 2–MSI for water quality monitoring at Alqueva reservoir," *Proceedings of IAHS*, vol. 380, pp. 73–79, 2018.

[18] M. H. Khalili and M. Hasanlou, "Harmful algal blooms monitoring using SENTINEL-2 satellite images," in *Proceedings of The International Archives of Photogrammetry, Remote Sensing and Spatial Information Sciences*, vol. XLII-4/W18, pp. 609–613, Karaj, Iran, 2019.

[19] G. Alba, F. Anabella, S. Marcelo et al., "Spectral monitoring of algal blooms in an eutrophic lake using Sentinel-2," in *IGARSS 2019 - 2019 IEEE International Geoscience and Remote Sensing Symposium*, pp. 306–309, Yokohama, Japan, 2019.

[20] T. Cecchi, "Analysis of volatiles organic compounds in Venice lagoon water reveals COVID 19 lockdown impact on microplastics and mass tourism related pollutants," *Science of the Total Environment*, vol. 783, no. 20, p. 146951, 2021.

[21] P. Silva, M. Ávila, and M. Gonçalves, "Air and water quality improvement during COVID-19 lockdown," *Proceedings of the 7th International Conference on Geographical Information Systems Theory, Applications and Management*, C. Grueau, R. Laurini, and L. Ragia, Eds., pp. 109–115, 2021.

[22] Orden TMA/419/2020, *Ministerio de Transportes, Movilidad y Agenda Urbana «BOE» núm. 141, de 19 de mayo de 2020 Referencia: BOE-A-2020-5125*, Ministerio de Transportes, Movilidad y Agenda Urbana, Madrid, 2020.

[23] Orden TMA/258/2020, *Ministerio de Transportes, Movilidad y Agenda Urbana «BOE» núm. 76, de 20 de marzo de 2020 Referencia: BOE-A-2020-3894*, Boletín Oficial del Estado 76, Ministerio de Transportes, Movilidad y Agenda Urbana, Madrid, 2020.

[24] T. Oguz, D. Macias, J. Garcia-Lafuente, A. Pascual, and J. Tintore, "Fueling plankton production by a meandering frontal jet: a case study for the Alboran Sea (Western Mediterranean)," *PLoS One*, vol. 9, no. 11, p. e111482, 2014.

[25] Esa sentinel online, "Sentinel-2, Sentinel Products," 2020, https://sentinel.esa.int/web/sentinel/missions/sentinel-2.

[26] Esa sentinel online, "Level-1," 2020, https://sentinel.esa.int/web/sentinel/user-guides/sentinel-2-msi/processing-levels/level-1.

[27] M. Sozzi, F. Marinello, A. Pezzuolo, and L. Sartori, "Benchmark of satellites image services for precision agricultural use," in *Proceedings of the AgEng conference*, pp. 8–11, Wageningen, The Netherlands, 2018.

[28] Copernicus open access hub, "Home," 2020, https://scihub.copernicus.eu/dhus/#/home.

[29] Q. Vanhellemont and K. Ruddick, "Acolite for Sentinel-2: aquatic applications of MSI imagery," *In Proceedings of the 2016 ESA Living Planet Symposium*, L. Ouwehand, Ed., , pp. 9–13, Prague, Czech Republic, 2016.

[30] Q. Vanhellemont, "Adaptation of the dark spectrum fitting atmospheric correction for aquatic applications of the Landsat and Sentinel-2 archives," *Remote Sensing of Environment*, vol. 225, pp. 175–192, 2019.

[31] ESRI ArcGIS Pro, 2020, https://pro.arcgis.com/es/pro-app/get-started/install-and-sign-in-to-arcgis-pro.htm.

[32] ARCGIS Desktop, "Mosaic to new raster," 2020, https://desktop.arcgis.com/en/arcmap/latest/tools/data-management-toolbox/mosaic-to-new-raster.htm.

[33] ARCGIS Desktop, "Raster calculator," 2020, https://desktop.arcgis.com/es/arcmap/latest/tools/spatial-analyst-toolbox/raster-calculator.htm.

[34] E. T. Slonecker, D. K. Jones, and B. A. Pellerin, "The new Landsat 8 potential for remote sensing of colored dissolved organic matter (CDOM)," *Marine Pollution Bulletin*, vol. 107, no. 2, pp. 518–527, 2016.

[35] J. Chen, W. Zhu, Y. Q. Tian, Q. Yu, Y. Zheng, and L. Huang, "Remote estimation of colored dissolved organic matter and chlorophyll-a in Lake Huron using Sentinel-2 measurements," *Journal of Applied Remote Sensing*, vol. 11, no. 3, p. 036007, 2017.

[36] J. Chen, W. Zhu, Y. Q. Tian, and Q. Yu, "Monitoring dissolved organic carbon by combining Landsat-8 and Sentinel-2 satellites: case study in Saginaw River estuary, Lake Huron," *Science of the Total Environment*, vol. 718, p. 137374, 2020.

[37] S. Novoa, D. Doxaran, A. Ody et al., "Atmospheric corrections and multi-conditional algorithm for multi-sensor remote sensing of suspended particulate matter in low-to-high turbidity levels coastal waters," *Remote Sensing*, vol. 9, no. 1, p. 61, 2017.

[38] L. Kang, Y. He, L. Dai et al., "Interactions between suspended particulate matter and algal cells contributed to the reconstruction of phytoplankton communities in turbulent waters," *Water Research*, vol. 149, pp. 251–262, 2019.

[39] B. Nechad, A. Dogliotti, K. Ruddick, and D. Doxaran, "Particulate backscattering retrieval from remotely-sensed turbidity in various coastal and riverine turbid waters," *Proceedings of ESA Living Planet Symposium*, L. Ouwehand, Ed., p. 740, 2016.

[40] M. Chapalain, *Dynamique des matières en suspension en mer côtière: caractérisation, quantification et interactions sédiments/matière organique, [Ph.D. thesis]*, Université de Bretagne Occidentale Brest, 2019.

[41] A. Pérez-Ruzafa, S. Campillo, J. M. Fernández-Palacios et al., "Long-term dynamic in nutrients, chlorophyll a, and water quality parameters in a coastal lagoon during a process of eutrophication for decades, a sudden break and a relatively rapid recovery," *Frontiers in Marine Science*, vol. 6, p. 26, 2019.

[42] W. J. Moses, A. A. Gitelson, S. Berdnikov, V. Saprygin, and V. Povazhnyi, "Operational MERIS-based NIR-red algorithms for estimating chlorophyll-a concentrations in coastal waters – the Azov Sea case study," *Remote Sensing of Environment*, vol. 121, pp. 118–124, 2012.

[43] M. A. Warren, S. G. Simis, V. Martinez-Vicente et al., "Assessment of atmospheric correction algorithms for the Sentinel-2A MultiSpectral imager over coastal and inland waters," *Remote Sensing of Environment*, vol. 225, pp. 267–289, 2019.

[44] N. Pahlevan, B. Smith, J. Schalles et al., "Seamless retrievals of chlorophyll-a from Sentinel-2 (MSI) and Sentinel-3 (OLCI) in inland and coastal waters: a machine-learning approach," *Remote Sensing of Environment*, vol. 240, p. 111604, 2020.

[45] C. J. Gobler, "Climate change and harmful algal blooms: insights and perspective," *Harmful Algae*, vol. 91, p. 101731, 2020.

[46] G. A. Carvalho, P. J. Minnett, V. F. Banzon, W. Baringer, and C. A. Heil, "Long-term evaluation of three satellite ocean color algorithms for identifying harmful algal blooms (Karenia brevis) along the west coast of Florida: a matchup assessment," *Remote Sensing of Environment*, vol. 115, no. 1, pp. 1–18, 2011.

[47] M. W. Matthews, S. Bernard, and L. Robertson, "An algorithm for detecting trophic status (chlorophyll-a), cyanobacterial-dominance, surface scums and floating vegetation in inland and coastal waters," *Remote Sensing of Environment*, vol. 124, pp. 637–652, 2012.

[48] Junta de Andalucia Consejería de Agricultura, Ganaderia, Pesca Y Desarrollo Sostenible, "Temperaturas y precipitaciones semanales AEMET," 2020, https://www.juntadeandalucia.es/organismos/agriculturaganaderiapescaydesarrollosostenible/servicios/estadistica-cartografia/estadisticas-agricolas/paginas/estadisticas-aemet.html.

[49] C. E. Binding, A. Zastepa, and C. Zeng, "The impact of phytoplankton community composition on optical properties and satellite observations of the 2017 western Lake Erie algal bloom," *Journal of Great Lakes Research*, vol. 45, no. 3, pp. 573–586, 2019.

[50] E. Organelli, A. Bricaud, D. Antoine, and A. Matsuoka, "Seasonal dynamics of light absorption by chromophoric dissolved organic matter (CDOM) in the NW Mediterranean Sea (BOUSSOLE site)," *Deep Sea Research Part I: Oceanographic Research Papers*, vol. 91, pp. 72–85, 2014.

[51] R. El Hourany, A. Fadel, E. Gemayel, M. Abboud-Abi Saab, and G. Faour, "Spatio-temporal variability of the phytoplankton biomass in the Levantine basin between 2002 and 2015 using MODIS products," *Oceanologia*, vol. 59, no. 2, pp. 153–165, 2017.

[52] P. Cresson, S. Ruitton, M. F. Fontaine, and M. Harmelin-Vivien, "Spatio-temporal variation of suspended and sedimentary organic matter quality in the Bay of Marseilles (NW Mediterranean) assessed by biochemical and isotopic analyses," *Marine Pollution Bulletin*, vol. 64, no. 6, pp. 1112–1121, 2012.

[53] J. Fabres, A. Calafat, A. Sanchez-Vidal, M. Canals, and S. Heussner, "Composition and spatio-temporal variability of particle fluxes in the Western Alboran Gyre, Mediterranean Sea," *Journal of Marine Systems*, vol. 33, pp. 431–456, 2002.

[54] Autoridad Portuaria de la Bahía de Algeciras, "Estadísticas," 2020, https://www.apba.es/estadisticas.

[55] Historical AIS Data Services, 2020, https://www.vesselfinder.com/historical-ais-data#traffic-density.

[56] Puerto de Malaga, "Información de atraques," 2020, https://www.puertomalaga.com/es/informacion-atraques/.

[57] J. Isern-Fontanet, E. García-Ladona, J. A. Jiménez-Madrid et al., "Real-time reconstruction of surface velocities from satellite observations in the Alboran Sea," *Remote Sensing*, vol. 12, no. 4, p. 724, 2020.

[58] A. G. Gómez, P. F. Valdor, B. Ondiviela, J. L. Díaz, and J. A. Juanes, "Mapping the environmental risk assessment of marinas on water quality: the atlas of the Spanish coast," *Marine Pollution Bulletin*, vol. 139, pp. 355–365, 2019.

[59] L. Sipelgas, R. Uiboupin, A. Arikas, and L. Siitam, "Water quality near Estonian harbours in the Baltic Sea as observed from entire MERIS full resolution archive," *Marine Pollution Bulletin*, vol. 126, pp. 565–574, 2018.

[60] R. Kudela, E. Berdalet, and E. Urban, *Harmful Algal Blooms: A Scientific Summary for Policy Makers*, 2015.

[61] W. Ouellette and W. Getinet, "Remote sensing for marine spatial planning and integrated coastal areas management: achievements, challenges, opportunities and future prospects," *Remote Sensing Applications: Society and Environment*, vol. 4, pp. 138–157, 2016.

[62] M. A. Burford, D. P. Hamilton, and S. A. Wood, "Emerging HAB research issues in freshwater environments," in *Global Ecology and Oceanography of Harmful Algal Blooms. Ecological Studies (Analysis and Synthesis)*, P. Glibert, E. Berdalet, M. Burford, G. Pitcher, and M. Zhou, Eds., vol. 232, pp. 381–402, Springer, Cham., Switzerland AG, 2018.

[63] K. Shi, Y. Zhang, B. Qin, and B. Zhou, "Remote sensing of cyanobacterial blooms in inland waters: present knowledge and future challenges," *Science Bulletin*, vol. 64, no. 20, pp. 1540–1556, 2019.

[64] J. L. Caparrós-Martínez, N. Rueda-Lópe, J. Milán-García, and J. de Pablo Valenciano, "Public policies for sustainability and water security: the case of Almeria (Spain)," *Global Ecology and Conservation*, vol. 23, p. e01037, 2020.

[65] D. A. Haith and J. V. Dougherty, "Nonpoint source pollution from agricultural runoff," *Journal of the Environmental Engineering Division*, vol. 102, no. 5, pp. 1055–1069, 1976.

[66] R. C. Griffin and D. W. Bromley, "Agricultural runoff as a nonpoint externality: a theoretical development," *American Journal of Agricultural Economics*, vol. 64, no. 3, pp. 547–552, 1982.

[67] J. Vymazal and T. Březinová, "The use of constructed wetlands for removal of pesticides from agricultural runoff and drainage: a review," *Environment International*, vol. 75, pp. 11–20, 2015.

[68] Q. Li, T. Wang, Z. Zhu et al., "Using hydrodynamic model to predict PFOS and PFOA transport in the Daling River and its tributary, a heavily polluted river into the Bohai Sea, China," *Chemosphere*, vol. 167, pp. 344–352, 2017.

[69] T. Matos, C. L. Faria, M. S. Martins, R. Henriques, P. A. Gomes, and L. M. Goncalves, "Development of a cost-effective optical sensor for continuous monitoring of turbidity and suspended particulate matter in marine environment," *Sensors*, vol. 19, no. 20, p. 4439, 2019.

[70] S. Sendra, L. Parra, J. Lloret, and J. M. Jiménez, "Oceanographic multisensor buoy based on low cost sensors for Posidonia meadows monitoring in Mediterranean Sea," *Journal of Sensors*, vol. 2015, Article ID 920168, 23 pages, 2015.